J Mater Sci (2007) 42:4177–4182
DOI 10.1007/s10853-006-0678-3

A multi-scaled model for the fracture toughness of an aluminum alloy

Min Song · Kang Hua Chen · Xiong Wei Qi · Lan Ping Huang

Received: 8 January 2006 / Accepted: 17 July 2006 / Published online: 9 March 2007

Abstract A multi-scaled model for the fracture toughness of an aluminum alloy has been developed that agrees well with the experimental data. It has been shown that fracture toughness decreases as the volume fraction of the first-class (related to microconstituents/inclusions) and second-class (related to second phase precipitates) microcracks increase, with the first-class microcracks have greater and more obvious effects. Thus, decreasing the volume fraction of the microconstituents (normally Fe and Si impurities) can decrease the volume fraction of the first-class microcracks and help improve the fracture toughness. At the same time, decreasing the volume fraction of the precipitates along the grain boundaries can also improve the fracture toughness by decreasing the volume fraction of the second-class microcracks.

Introduction

Aluminum alloys are widely used as structural materials nowadays. However, the improvement in strength will usually decrease the fracture toughness of the alloys, thereby limiting their applications. Thus, extensive research [1–10] has been performed to examine the relationship between fracture toughness and microstructure. These studies have indicated that the coarse microconstituents/inclusions and finer precipitates/dispersoids (large-sized precipitates) along grain boundaries are initiation sites for fracture and can be treated as pre-existing microcracks. Based on the above assumption, several models [6–9, 11] have been developed to describe the relationship between fracture toughness and the volume fraction of the microcracks. These models assume that the microcracks have the same size for simplicity in mathematics. However, the microcracks caused by the coarse microconstituents and by the fine precipitates have various sizes and thus the developed models are oversimplified. The coarse microconstituents result from the presence of Fe and Si impurities or major alloying elements, and are normally 1–5 vol.% in volume fraction and 1–30 μm in size, whereas the fracture at grain boundaries results from the finer precipitates caused by heterogeneous precipitation along the grain boundaries. These precipitates are normally 0.1–0.5 μm in size [6]. This paper, as a first step, developed a multi-scaled model (including two types of microcracks described above) to describe the relationship between fracture toughness and the volume fraction of the coarse microconstituents and fine precipitates.

Model

Figure 1a and b are typical micrographs showing the microcracks caused by both microconstituents and finer precipitates after straining [12] in Al–Cu–Mg alloy. Since the coarse microconstituents will fracture readily under loading, they have been treated as the first-class

M. Song (✉) · K. H. Chen · X. W. Qi · L. P. Huang
State Key Laboratory of Powder Metallurgy, Central South University, Changsha 410083, PR China
e-mail: Min.Song.Th05@Alum.Dartmouth.ORG

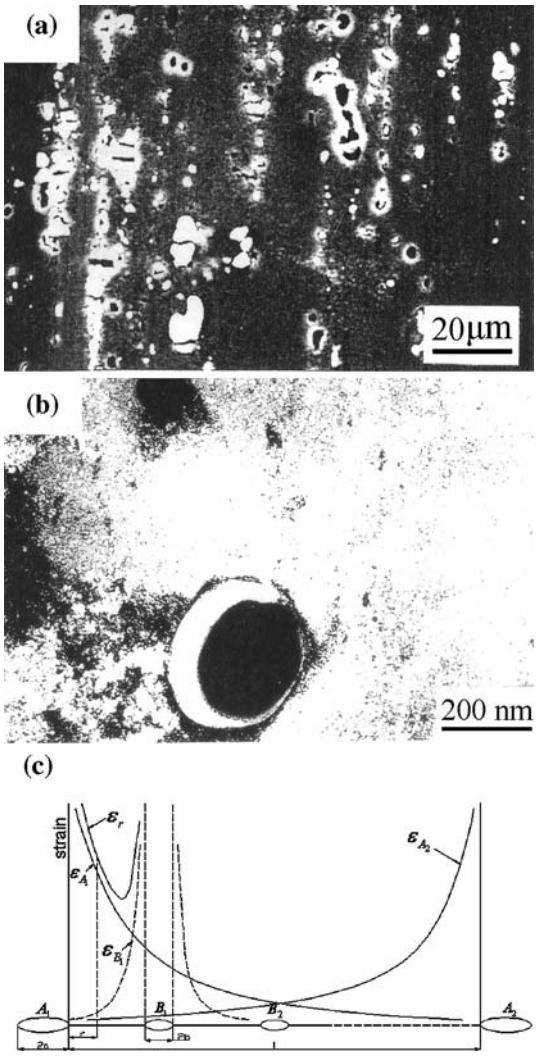

Fig. 1 Microcracks caused by (**a**) fracture of the coarse micro-constituents and (**b**) the decohesion of the precipitates from the matrix during deformation in Al–Cu–Mg alloy (from Ref. [12]), (**c**) geometric model for fracture toughness

microcracks directly, with dimension of $2a$. Normally, precipitate-free zones exist along the grain boundaries, and have observed by researchers [1, 3]. These zones are very soft, and the plastic strain will be highly localized during deformation. Thus, the intergranular precipitates will promote decohesion from the grain boundaries and initiate microcracks. These microcracks have been termed second-class microcracks, with dimension of $2b$. For simplicity, assume that the microcracks are distributed uniformly, as shown in Fig. 1c.

First, we assume only one second-class microcrack (B_1) exists in between two neighboring first-class microcracks (A_1 and A_2). Thus, at a distance, r (r is the distance between microcracks A_1 and B_1), ahead of microcrack A_1, the strain tensor caused by microcracks A_1, A_2 and B_1, is given by [13, 14]:

$$\varepsilon_{ij}^{A1} = \alpha\varepsilon_y \left[\frac{J_{A1}}{\alpha\varepsilon_y\sigma_y I_n r}\right]^{n/(1+n)} \tilde{\varepsilon}_{ij}(\theta) \tag{1}$$

$$\varepsilon_{ij}^{A2} = \alpha\varepsilon_y \left[\frac{J_{A2}}{\alpha\varepsilon_y\sigma_y I_n (l-r)}\right]^{n/(1+n)} \tilde{\varepsilon}_{ij}(\theta) \tag{2}$$

$$\varepsilon_{ij}^{B1} = \alpha\varepsilon_y \left[\frac{J_{B1}}{\alpha\varepsilon_y\sigma_y I_n (l/2-b-r)}\right]^{n/(1+n)} \tilde{\varepsilon}_{ij}(\theta) \tag{3}$$

where J is the J-integral, ε_y the yield strain, σ_y the yield stress, n the inverse of the strain hardening exponent, α the material constant in the Ramberg–Osgood constitutive relation [15], and I_n and $\tilde{\varepsilon}_{ij}(\theta)$ are the normalized parameter in the HRR-field [13, 14].

The J-integral can be separated into elastic (J_e) and plastic (J_p) components. For an aluminum alloy, J_e is much smaller than J_p, and can be ignored. Thus the J-integral is given by [16]:

$$J_{A1} \approx J_{A1p} = \frac{0.405\pi h\sigma_y a[\varepsilon_p]^{(1+n)/n}}{[\alpha\varepsilon_y]^{1/n}} \tag{4}$$

$$J_{A2} \approx J_{A2p} = \frac{0.405\pi h\sigma_y a[\varepsilon_p]^{(1+n)/n}}{[\alpha\varepsilon_y]^{1/n}} \tag{5}$$

$$J_{B1} \approx J_{B1p} = \frac{0.405\pi h\sigma_y b[\varepsilon_p]^{(1+n)/n}}{[\alpha\varepsilon_y]^{1/n}} \tag{6}$$

where ε_p is plastic strain, $h = \frac{3}{2\sqrt{1+3/n}}$. Substituting Eqs. 4, 5 and 6 into Eqs. 1, 2 and 3, respectively, leads to

$$\varepsilon_{ij}^{A1} = Q \cdot \varepsilon_p \cdot \left(\frac{a}{r}\right)^{n/(1+n)} \tag{7}$$

$$\varepsilon_{ij}^{A2} = Q \cdot \varepsilon_p \cdot \left(\frac{a}{l-r}\right)^{n/(1+n)} \tag{8}$$

$$\varepsilon_{ij}^{B1} = Q \cdot \varepsilon_p \cdot \left(\frac{b}{l/2-b-r}\right)^{n/(1+n)} \tag{9}$$

where $Q = \alpha\varepsilon_y \left[\frac{0.405\pi h}{\alpha\varepsilon_y I_n}\right]^{n/(1+n)} \tilde{\varepsilon}_{ij}(\theta)$. Adding Eqs. 7, 8 and 9 leads to

$$\varepsilon_p = \frac{\varepsilon_{ij}}{Q} \cdot \left[\frac{r}{a}\right]^{n/(1+n)} \cdot \frac{1}{1 + \left[\frac{r}{l-r}\right]^{n/(1+n)} + \left[\frac{rb}{a}\right]^{n/(1+n)} \cdot \left[\frac{1}{l/2-b-r}\right]^{n/(1+n)}} \quad (10)$$

If there are m second-class microcracks distributed uniformly between two neighboring first-class microcracks A_1 and A_2, Eq. 10 changes to

$$\varepsilon_p = \frac{\varepsilon_{ij}}{Q} \cdot \left[\frac{r}{a}\right]^{n/(1+n)} \cdot \frac{1}{1 + \left[\frac{r}{l-r}\right]^{n/(1+n)} + \left[\frac{rb}{a}\right]^{n/(1+n)} \cdot \sum_{z=1}^{m} \left[\frac{1}{zl/(1+m)-b-r}\right]^{n/(1+n)}} \quad (11)$$

When the local effective strain, ε_{ij}, at location r in the matrix ligament reaches the matrix fracture strain, ε_{mf}, the plastic strain, ε_p, reaches the nominal fracture strain, ε_f, or tensile ductility at the onset of fracture. Thus, Eq. 11 changes to

$$\varepsilon_f = \frac{\varepsilon_{mf}}{Q} \cdot \left[\frac{r}{a}\right]^{n/(1+n)} \cdot \frac{1}{1 + \left[\frac{r}{l-r}\right]^{n/(1+n)} + \left[\frac{rb}{a}\right]^{n/(1+n)} \cdot \sum_{z=1}^{m} \left[\frac{1}{zl/(1+m)-b-r}\right]^{n/(1+n)}} \quad (12)$$

Based on the criterion that fracture will occur when the local strain ahead of the main crack exceeds the critical value ε_c^*, an expression has been established to relate the fracture toughness of the aluminum alloy to the yield strength , the strain hardening exponent n, Young's modulus and ε_c^* [17]:

$$K_{IC} = \sqrt{\frac{2CE\varepsilon_c^*\sigma_y}{(1-\nu^2)n^2}} \quad (13)$$

where C is a constant of ~0.025 and ν is Poisson's ratio. It has been suggested [18] that ε_c^* was probably half of the true strain ε_f, and some experimental results [17] indicated that this is a reasonable first approximation. Thus, we substitute ε_c^* with $\varepsilon_f/2$ into Eq. 13:

$$K_{IC} = \sqrt{\frac{CE\sigma_y\varepsilon_{mf}}{Qn^2(1-\nu^2)} \cdot \left[\frac{r}{a}\right]^{n/(1+n)} \cdot \frac{1}{1 + \left[\frac{r}{l-r}\right]^{n/(1+n)} + \left[\frac{rb}{a}\right]^{n/(1+n)} \cdot \sum_{z=1}^{m} \left[\frac{1}{zl/(1+m)-b-r}\right]^{n/(1+n)}}} \quad (14)$$

For a cubic array, the volume fraction (f) of the microcracks is a function of mean radius (a and b) and the interspacing λ:

$$f_{total} = f_{first} + f_{second} = 2\pi\left[k_A\left(\frac{a}{\lambda_a}\right)^3 + k_B\left(\frac{b}{\lambda_b}\right)^3\right] \quad (15)$$

where k is the aspect ratio of microcracks. For second-class microcracks caused by spherical precipitates, k_B is 1. For first-class microcracks caused by disk-like microconstituents, k_A is defined as the ratio between the radius of the plate plane and the half height of the disc, whereas for first-class microcracks caused by spherical microconstituents, k_A is 1.

If we define $(K_{IC})_0$ as the reference fracture toughness, the normalized fracture toughness can be expressed as

$$R = K_{IC}/(K_{IC})_0 \quad (16)$$

We assume that when the local effective strain in the middle of the matrix ligament (between microcracks A_1 and B_1) reaches the matrix fracture strain, the plastic strain reaches the nominal fracture strain and the material starts to fracture. Since the volume fraction of the two types of microcracks cannot be set to zero at the same time in Eqs. 12 and 14, in this study, it is assumed that the material is free of microcracks when the volume fraction of the first-class microcracks is as low as 0.01% and the volume fraction of the second-class microcracks is zero.

Model predictions and discussion

Effect of the volume fraction and size of the microconstituents on the normalized fracture toughness

Figure 2 shows the effect of the volume fraction of the microconstituents on the normalized fracture toughness (assume no second-class microcracks exist). The reference was defined as the microconstituent volume fraction of 0.01%. Four values of k_A have been illustrated: 0.5, 1, 2 and 5 (a = 10 μm). It can be seen

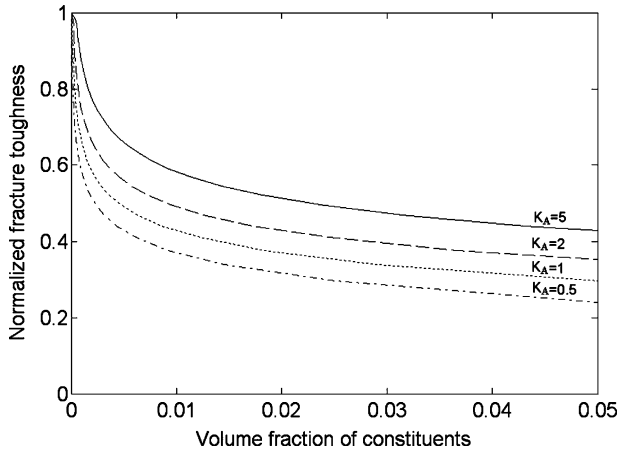

Fig. 2 Effect of the volume fraction of the microconstituents on the normalized fracture toughness

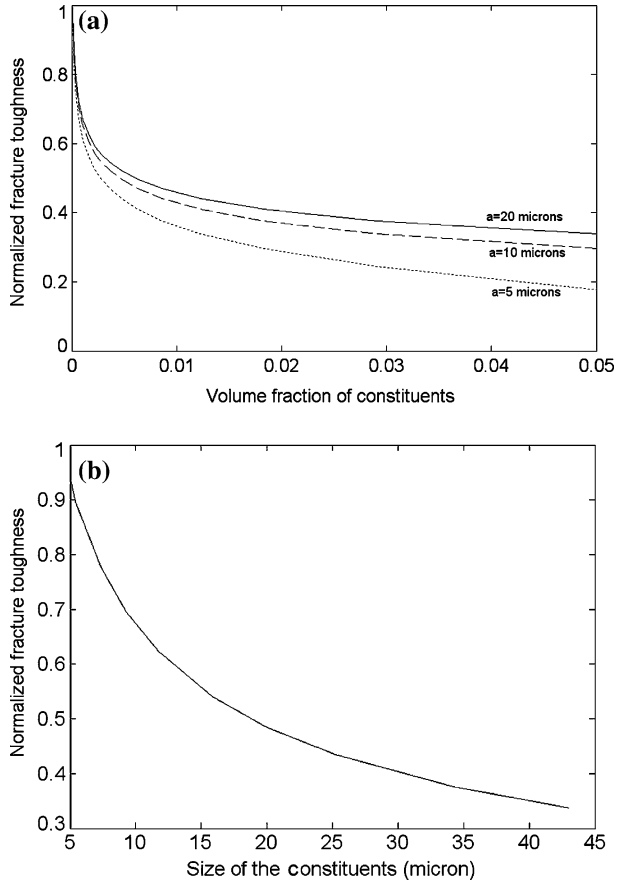

Fig. 3 Effect of the size of the microconstituents on the normalized fracture toughness (note: in Fig. 3b, the distance between two microconstituents remains constant as 86 μm)

that no matter what the value k_A is, the normalized fracture toughness decreases as the volume fraction of the microconstituents increases. This indicated that an increase in impurities (promoting the formation of coarse inclusions), or more coarse microconstituents will degrade the fracture toughness of aluminum alloy. Thus, reducing the inclusion content (reducing impurities) is an effective way to improve the fracture resistance. It should be noted that the increase in k_A value will also improve the fracture toughness. A sharp crack can cause a high stress concentration at a crack tip if disk-like cracks are perpendicular to the stress direction rather than along the stress direction. Thus, the higher the k_A value, the higher is the fracture toughness.

The effect of the size of the microconstituents on the normalized fracture toughness is illustrated in Fig. 3. It can be seen from Fig. 3a that decreasing the size of the microconstituents degrades the normalized fracture toughness for a constant volume fraction, since decreasing the size of the microconstituents increases the number and decreases the distance between two neighboring microconstituents. Actually, if the volume fraction of the microconstituents remains constant, the distance decreases linearly with the size of the microconstituent. Decreasing the size of the microconstituents will improve the fracture resistance dramatically if the distance between two neighboring microconstituents remains constant, which is illustrated in Fig. 3b.

Effect of precipitates along the grain boundaries on the normalized fracture toughness

From Fig. 1b, it is obvious that second-class microcracks are normally initiated from the decohesion of fine precipitates from the matrix (normally along the grain boundaries) during deformation. Figure 4 shows the effect of the appearance of the second-class microcracks on the normalized fracture toughness (some previous experimental data [19] for Al–Cu–Mg alloy are also included). Since the coarse microconstituents and the stable precipitates (θ: Al_2Cu) along the grain boundaries in Al–Cu–Mg alloy are spherical or near spherical [12], we then assume that both k_A and k_B are 1. The reference was also set as the volume fraction of the microconstituents is as low as 0.01% and the volume fraction of the second-class microcracks is zero. The sizes of the coarse microconstituents and the large-sized precipitates were set as 20 and 0.5 μm, respectively.

It can be seen that the normalized fracture toughness decreases as the volume fraction of the microconstituents increases, as observed in Fig. 2. It can also be seen that the normalized fracture toughness decreases with the appearance of the second-class microcracks. As the proportion of second-class

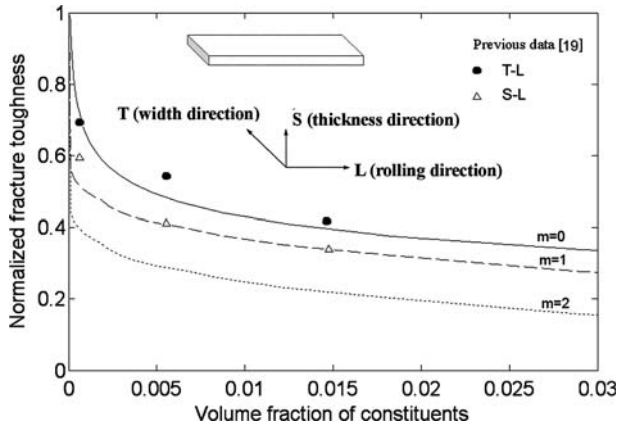

Fig. 4 The effect of the appearance of the second-class microcracks on the normalized fracture toughness (T, L and S indicated the directions of the rolled plate, *m* is defined as the number of the second-class microcracks between two neighboring first-class microcracks)

microcracks increases, the fracture toughness decreases (comparing $m = 0$, $m = 1$ and $m = 2$ in Fig. 4, m is defined as the number of the second-class microcracks between two neighboring first-class microcracks). Figure 4 also indicates that the main reason for the decrease in fracture toughness is due to the first-class microcracks (associated with the coarse microconstituents). The modeling values agree well with the experimental data when $m = 0$ and $m = 1$, which implies that the second-class microcracks only have minor effects on the fracture toughness of a rolled plate. Actually, for an aluminum alloy with coarse microconstituents, the plastic stain concentration along the interface between the microconstituents and matrix is highly localized and the microcracks caused by fracture of the microconstituents propagate very easily during deformation before the decohesion of the finer precipitates from the matrix occurs. Thus, although normally more than one precipitate is distributed between two neighboring constituents, only one or two will separate from the grain boundaries with the least integrated strength. It should be noted that the rolled plate was largely recrystallized, and that it has a much greater fracture toughness along T–L plane than along S–L plane (S, T and L indicate thickness direction, width direction and rolling direction, respectively). This is reasonable, since after rolling, the coarse microconstituents in the processed aluminum alloys are usually ellipsoidal in shape with the larger axis being parallel to the roll direction. In the subsequent testing, when the loading axis is parallel to the larger axis of the microconstituents, the defined aspect ratio of the microconstituents is greater than unity; when the loading axis is parallel to the short axis of the microconstituents, the defined aspect ratio of the microconstituents is less than unity. According to the model prediction in Fig. 2, the fracture toughness in the latter case is inferior to that in the former case, because the ligament between two most neighboring constituents is shorter in the latter case. The shorter ligament implies that two microcracks caused by the microconstituents are more easily connected during deformation.

Figure 5 shows the effect of the volume fraction of the second-class microcracks on the normalized fracture toughness. The reference was set as the volume fraction of the microconstituents is 1%. It can be seen that the normalized fracture toughness decreases as the volume fraction of the second-class microcracks increases. A previous study [20] indicated that quenching rate has strong effect on the volume fraction of large-sized precipitates (dispersoids) in a 7050 aluminum alloy. The volume fraction of these large precipitates formed as a result of a fast quenching rate (850 K s^{-1}) is about 0.5%, whereas a slow quenching rate (7 K s^{-1}) results in a volume fraction of about 1.5%. These different quenching rates affect the fracture toughness. The transferred normalized fracture toughness data from Ref. [20] are also included in Fig. 5. It can be seen that the values predicted by the model agree well with the experimental data.

Figures 4 and 5 indicated that the volume fraction of the second-class microcracks will also affect the fracture toughness of aluminum alloys. The second-class microcracks are caused by the decohesion of the intergranular precipitates from grain boundaries during deformation. However, since the size of these precipitates and the stress concentration at the interface between these precipitates and the matrix are much smaller than that of the coarse microconstituents, not

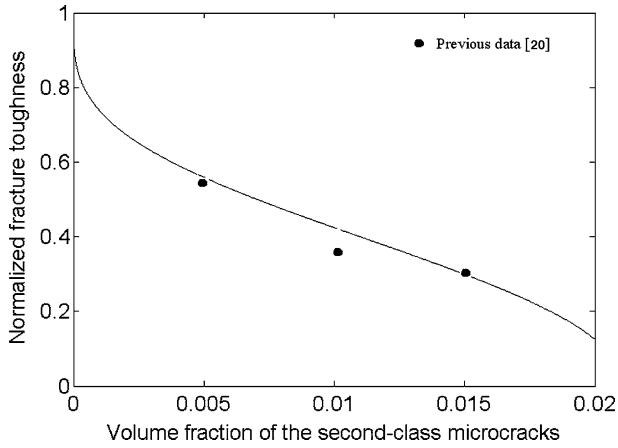

Fig. 5 The effect of the volume fraction of the second-class microcracks on the normalized fracture toughness

all of them will separate from matrix during deformation, and they will have a minimal effect on the fracture toughness in contrast to that of the coarser microconstituents. Changing the heat-treatment procedure can decrease the volume fraction of the precipitates and thus improve the fracture toughness.

Conclusions

A multi-scaled model for fracture toughness of aluminum alloys has been developed, and it agrees well with the experimental data. The model indicated some important results:

(1) The fracture toughness decreases with the increase in volume fraction of the first-class and second-class microcracks.
(2) Decreasing Fe and Si impurities will decrease the volume fraction of the coarse microconstituents and help improve the fracture toughness of Al–Cu–Mg alloy.
(3) Proper heat-treatment processing can decrease the volume fraction of the precipitates along the grain boundaries, and help improve the fracture toughness by decreasing the volume fraction of the second-class microcracks.

Acknowledgement This work was supported by the Chinese National Key Fundamental Research Project (2005CB623704) on Al.

References

1. Ludtka GM, Laughlin DE (1982) Metall Trans A 13A:411
2. Deshpande NU, Gokhale AM, Denzer DK, Liu J (1998) Metall Trans A 29A:1191
3. Hornbogen E, Gräf M (1977) Acta Metall 25:877
4. Jata KV, Starke EA (1986) Metall Trans A 17A:1011
5. Liu G, Zhang GJ, Ding XH, Sun J, Chen KH (2002) The Chin J Nonferrous Metals 12:706
6. Hornbogen E, Starke EA (1993) Acta Metall Mater 41:1
7. Gokhale AM, Deshpande NU, Denzer DK, Liu J (1998) Metall Trans A 29A:1203
8. Liu G, Zhang GJ, Ding XD, Sun J, Chen KH (2004) Metall Trans A 35A:1725
9. Roven HJ (1992) Scripta Metall Mater 26:1383
10. Liu G, Sun J, Nan CW, Chen KH (2005) Acta Mater 53:3459
11. Chan KS (1995) Acta Metall Mater 43:4325
12. Liu G, Zhang GJ, Ding XD, Sun J, Chen KH (2003) Mater Sci Technol 19:887
13. Hutchinson JW (1968) J Mech Phys Solids 16:13
14. Rice JR, Rosengrn GF (1968) J Mech Phys Solids 16:1
15. Kanninen MF, Popelar CH (1985) Advanced fracture mechanics. Oxford University Press, New York, p 300
16. Dowling NE (1987) Eng Fract Mech 26:333
17. Garrett GG, Knott JF (1978) Metall Trans A 9A:1187
18. Hahn GT, Rosenfield AR (1968) ASTM STP 432:5
19. Peel CJ, Forsyth PJE (1970) Technical report 70162. Royal Aircraft Establishment, Farnborough, UK
20. Dumont D, Deschamps A, Brechet Y (2003) Mater Sci Eng A 356:326